Research Article | Vol. 29, No. 7 / 29 March 2021 / Optics Express 10863
Optics EXPRESS

Transient mid-IR nonlinear refraction in air

SALIMEH TOFIGHI,[1,4] NATALIA MUNERA,[1,2,4] MATTHEW REICHERT,[3] DAVID J. HAGAN,[1,*] AND ERIC W. VAN STRYLAND[1]

[1]CREOL, the College of Optics and Photonics, University of Central Florida, Orlando, FL 32816, USA
[2]Escuela de Fisica, Universidad Nacional de Colombia-Medellin, Medellin 050034, Colombia
[3]Currently with CACI International, Inc., Florham Park, NJ 07932, USA
[4]These authors contributed equally to this work
[*]hagan@creol.ucf.edu

Abstract: We use the polarization-sensitive, time-resolved Beam-Deflection technique to measure the nonlinear refraction of air, exciting in both the near and mid-IR and probing in the mid-IR. This gives us the first measurements for air using both excitation and probe in the mid-IR, and we find no dispersion of the bound-electronic nonlinear refractive index, $n_{2,el}(\lambda_p;\lambda_e)$, assuming, as has been shown earlier, that the nuclear rotational nonlinear refraction is nearly dispersionless. From these data, we can model the pulsewidth dependence of the effective nonlinear refractive index, $n_{2,eff}$, i.e., as would be measured by a single beam. Interestingly, $n_{2,eff}$ is maximized for a pulsewidth of approximately 0.5 ps. The position of this maximum is nearly independent of pressure while its magnitude decreases with increasing pressure and temperature. From the measurements and modeling, we predict the nonlinear refraction in the atmosphere at different altitudes.

1. Introduction

The existence of a transparency window in the Mid-IR [1] has raised considerable interest in atmospheric propagation of short Mid-IR laser pulses. Propagation of high-power self-guided, diffraction-resistant laser filaments in the atmosphere has attracted attention in remote sensing and LIDAR [2–8]. The directional behavior of filaments, including their directional backscatter makes them favorable for LIDAR applications [7]. In addition, Mid-IR filamentation in air can be used to detect pollutants and aerosols [6]. Furthermore, high harmonic generation [9] and broadband supercontinuum generation [5] are other applications of high-power short laser pulses in the Mid-IR. All these applications necessitate knowledge of nonlinear refraction (NLR) of air for Mid-IR spectral ranges. Most of the experimental studies on the nonlinear propagation of short laser pulses in air have been done for the visible and near IR (NIR) ranges [10–12] and information in the Mid-IR spectral range is limited. Additionally, most measurements have used two beams of different wavelengths yielding the nondegenerate nonlinear refractive indices, which are functions of the two wavelengths of the excitation and probe beams. An exception is Pigeon *et al.* [13], who used degenerate four-wave mixing at a wavelength of 10 μm with picosecond laser pulses to measure the nonlinear refractive index of air and air constituents. In the experiments presented here, we also use excitation and probe beams of different frequencies; however, we make the first measurement in the Mid-IR using nearly degenerate beams. This allows us to make conclusions about the overall nonlinear refraction experienced by a single beam.

For this case of only a single beam, we define the nonlinear index change as:

$$\Delta n = n_{2,eff} I \tag{1}$$

where $n_{2,eff}$ includes the nearly instantaneous response due to bound electrons ($n_{2,el}$) a small and ultrafast response due to molecular vibrations ($n_{2,vib}$) and the molecular reorientational response

#414495 https://doi.org/10.1364/OE.414495
Journal © 2021 Received 11 Nov 2020; revised 12 Feb 2021; accepted 10 Mar 2021; published 23 Mar 2021

Optics EXPRESS

($n_{2,rot}$), and I is the irradiance of the beam. It is expected that $n_{2,el} \gg n_{2,vib}$ for any pulsewidth [14] and this is consistent with our initial calculations given in Sec. 6. Additionally, while in principle the vibrational and bound-electronic contributions are distinguishable because the relative polarization dependences are different [14], these angular differences are so small as to make them experimentally indistinguishable (at least for errors of a few %), unless pulses shorter than the vibrational period are used. So henceforth, we shall simply refer to the combined bound-electronic and vibrational contributions as $n_{2,el}$ to be consistent with previous publications [11,15–17].

In [13] $n_{2,el}$ and $n_{2,rot}$ could not be separately resolved because of the long pulse duration. In a different 2-beam experiment, Zahedpour *et. al.*, used single-shot supercontinuum spectral interferometry (SSSI) [18] to measure the nonlinear phase shift of air constituents using a weak visible supercontinuum probe with excitation in the Mid-IR [15,16]. In this paper, we use the time-resolved and polarization-sensitive Beam-Deflection (BD) technique [17] to measure the ultrafast $n_{2,el}$ of air, with different combinations of wavelengths including a near-degenerate experiment in the Mid-IR. Our analysis assumes, as has been verified previously by others, a very small dispersion of the reorientational response (<3% for either oxygen (O_2) or nitrogen (N_2)) in this spectral range [15,19,20]. Therefore, we ignore this dispersion in this paper.

Under these assumptions, we observe no dispersion in $n_{2,el}$, as can be expected for air whose constituents all have resonant absorption in the UV, far from the wavelengths used in these experiments [21]. The BD technique has several advantages over other techniques. In comparison to the optical Kerr effect (OKE) [22] and degenerate four-wave mixing [23] techniques it does not need a complicated optical heterodyne detection (OHD) system to measure the sign of the nonlinear refractive index, and the experimental implementation is simpler with respect to interferometric methods [18]. Being a 2-beam experiment, it is sensitive to the relative polarization of the two inputs, which is advantageous since it allows separation of the bound-electronic $n_{2,el}$ and the molecular reorientation effects based on symmetry. Additionally, the high sensitivity of BD allows us to directly measure the nonlinear phase shift of air for both NIR and Mid-IR excitation even though the signal varies as λ^{-1}.

Using our measurements, including the nearly degenerate Mid-IR data, we have calculated the pulsewidth dependence of the effective nonlinear refractive index encountered by a single beam [24,25]. This is discussed in Section 5. Our results show that for very short pulse durations ($\lesssim$ 10 fs) the contribution of the rotational nonlinearity becomes negligible leaving only the ultrafast $n_{2,el}$. As the pulsewidth increases the reorientational contribution to NLR becomes important and at considerably longer pulsewidths ($\gtrsim$ 4 ps, for air at 1 atm) it again becomes independent of pulsewidth. This is true for a wide range of pressure and temperature. However, we find a small maximum $n_{2,eff}$ for pulsewidths around 0.5 ps, which we attribute to the oscillatory behavior of the reorientational response function. Interestingly, as we will show, the maximum position remains near 0.5 ps [16], nearly independent of pressure and temperature, and thus nearly independent of altitude.

2. Theory

Nonlinear refraction, NLR, in molecular gases originates from the combination of an almost instantaneous bound-electronic response, a weak ultrafast vibrational Raman response (see Sec. 6) and a non-instantaneous field-induced reorientational Raman response [10,14,18]. The contribution of vibrational responses has been regarded as negligible in prior studies [10,11,15–18]. Shelton and Rice [12] estimate the steady state vibrational contribution to be <3~5% of the bound-electronic contribution. Because the vibrational periods for the major constituents of air N_2 and O_2 are 14 fs for N_2 and 21 fs for O_2, for pulses longer than ~50 fs the vibrational effect is essentially instantaneous. Therefore, as described earlier, we use $n_{2,el}$ to describe the combined bound-electronic and vibration contributions (see Sec. 6). Both N_2

Optics EXPRESS

and O_2 have anisotropic polarizabilities. We define the anisotropic polarizability, $\Delta\alpha$, as the difference in polarizabilities parallel and perpendicular to the molecular axis ($\Delta\alpha = \alpha_{\parallel} - \alpha_{\perp}$). In contrast, Argon, which makes up ~1% of the atmosphere, has $\Delta\alpha = 0$. An intense electric field will induce a time-dependent torque on the randomly oriented molecules and will rotate the largest polarizability axis toward the direction of the excitation polarization. This induces an index change. By probing the index change with different polarization combinations at different times we can measure the transient response of the NLR. The reorientational response is a rotational Raman contribution to the NLR [26–28]. If the laser pulse is short compared to the rotational periods, it excites all the allowed rotational Raman transitions simultaneously, which are approximately equally spaced, subject to the selection rule $\Delta J = \pm 2$ with J the rotational quantum number. As a result, molecules in different rotational states and rotating at different rates will periodically rephase, producing periodic pulsations of the refractive index known as reorientational revivals. After some time, the coherence between rotational levels decays because of collisions between gas molecules and centrifugal distortion that causes the comb-like spacing of Raman lines to become unequal, thus not continuing to add in phase, and consequently the revivals are suppressed. Revivals can be calculated as the ensemble average of the degree of alignment $\langle cos^2\theta(t)\rangle$, where $\theta(t)$ is measured with respect to the polarization of the excitation beam. We can calculate $\langle cos^2\theta(t)\rangle$, and as a result calculate the refractive index change due to the rotational Raman effect. The total nonlinear refraction at the probe wavelength λ_p due to the excitation at λ_e is the ultrafast contribution plus the reorientational contribution,

$$\Delta n_{total}(\lambda_p; \lambda_e, t) = 2n_{2,el}(\lambda_p; \lambda_e)I_e(t) + \Delta n_{rot}(t) = \Delta n_{el}(t) + \Delta n_{rot}(t) \tag{2}$$

where $I_e(t)$ is the excitation beam irradiance and $\Delta n_{rot}(t)$ is the change in the refractive index due to the molecular response, which is assumed to be wavelength independent [26,29]. The factor of 2 in the $\Delta n_{el}(t)$ in Eq. (2) is because of the interference of two beams doubling the phase change. There is no factor of 2 in the rotational term since the nonlinearity cannot follow the rapidly moving interference pattern in these nondegenerate experiments [30,31]. For a single beam experiment the factor of 2 is absent. Unlike the bound-electronic response, the reorientational response depends on the pulsewidth. The index change from the reorientational response due to the excitation is given by:

$$\Delta n_{rot}(t) = \int_{-\infty}^{t} R_{rot}(t - t')I_e(t')\mathrm{d}t', \tag{3}$$

where, $R_{rot}(t)$ is the molecular reorientational response function [24]. We find from this relation that for very short pulses, ~10 fs or shorter, the effects from the molecular reorientational contribution on $n_{2,eff}$ are negligible. However, for pulses longer than this, the contribution of the non-instantaneous molecular reorientation response must be considered. We report the dependence of the effective nonlinear refractive index, $n_{2,eff}$, on the pulsewidth in Section 5.

Using the density matrix formalism, the reorientational response for each molecular component can be calculated [18,26,29,32]:

$$\Delta n'_{rot}(t) = \frac{N}{2c\varepsilon_0^2 n_0^2}(\Delta\alpha)^2 \sum\nolimits_J T_J \int_{-\infty}^{t} I_e(t')\sin(\omega_{J,J-2}(t - t'))e^{-\Gamma_{J,J-2}(t-t')}\mathrm{d}t' \tag{4}$$

where N is the number density of molecules for each component of air, c the speed of light, ε_0 is the permittivity, n_0 the corresponding linear index which for all cases here is approximately unity, $\omega_{J,J-2} = 4\pi cB(2J - 1)$ is the corresponding rotational Raman frequency neglecting the centrifugal distortion, B is the rotational constant and J the rotational quantum number. The prime on $\Delta n'_{rot}$ indicates that it is for a single component of air. The total $\Delta n_{rot}(t)$ is given by summing over the weighted average of the air components. The decay of the revivals is characterized by a dephasing rate, $\Gamma_{J,J-2}$, which depends on intermolecular collisions. This decay

Optics EXPRESS

depends on pressure and is different for different J values. Values are given in Refs. [10,33]. In Eq. (4) T_J is a weighting factor given by [10,26];

$$T_J = \frac{2}{15\hbar}\frac{J(J-1)}{2J-1}(\rho_{JJ}^{(0)} - \rho_{J-2,J-2}^{(0)}). \tag{5}$$

Here $\hbar$ is the Planck constant and $\rho_{JJ}^{(0)}$ is the initial occupation probability of the rotational state J, which can be written as:

$$\rho_{JJ}^{(0)} = \frac{g_J e^{-\frac{E_J}{K_B T}}}{\sum_k g_k(2k+1)e^{-\frac{E_k}{K_B T}}} \tag{6}$$

where k_B is the Boltzmann constant and g_J is the weighting factor based on nuclear spin statistics for each molecule [34]. $E_J = 2\pi c\hbar BJ(J+1)$ is the rotational energy and T the temperature. For N_2 even J states have $g_J = 2/3$ and odd have $g_J = 1/3$, while for O_2 even J states have $g_J = 0$ and odd J states $g_J = 1$ [34].

Using Eqs. (3) and (4), the response function $R_{rot}(t)$ can be written as:

$$R_{rot}(t) = \Theta(t)\frac{N}{2c\varepsilon_0^2 n_0^2}(\Delta\alpha)^2 \sum_{J=0}^{\infty} T_J \sin(\omega_{J,J-2}t)e^{-\Gamma_{J,J-2}t}, \tag{7}$$

where the Heaviside function ($\Theta(t)$) ensures the response function obeys causality. Equation (7) shows that the response function of the molecular reorientational contribution to the NLR depends on $\Delta\alpha^2$. This is very useful, since the amplitude of the rotational response depends on these known values of $\Delta\alpha$. We can obtain a very simple relation allowing $n_{2,el}$ to be determined in terms of $\Delta\alpha$ [10] from Eqs. (2) and (4):

$$\frac{\Delta n_{el}}{\Delta n_{rot}} \propto \frac{n_{2,el}}{\Delta\alpha^2}, \tag{8}$$

thus, $\Delta\alpha$ serves as a self-reference for measuring $n_{2,el}$.

The final calculation that needs to be performed is a correlation of the probe pulse in time with the convolution of Eq. (3) where R_{rot} is replaced by the overall causal response function R_{Total} (bound electronic plus vibrational Raman, treated as a delta function, plus molecular reorientational). This results in the index change temporally averaged over the probe pulse,

$$\langle\Delta n(\tau)\rangle = \frac{1}{\int_{-\infty}^{\infty} I_p(t)dt}\int_{-\infty}^{\infty} dt\, I_p(t-\tau)\int_{-\infty}^{\infty} R_{Total}(t-t')I_e(t')\mathrm{d}t' \tag{9}$$

where I_p is the irradiance of the probe beam. It can be shown, most simply by taking Fourier transforms [35], that this is equivalent to the convolution of R_{Total} with the cross-correlation of the excitation and probe pulses [22,36]:

$$\langle\Delta n(\tau)\rangle = \frac{1}{\int_{-\infty}^{\infty} I_p(t)dt}\int_{-\infty}^{\infty} dt\, R_{Total}(\tau-t)\int_{-\infty}^{\infty} I_e(t')I_p(t'-t)\mathrm{d}t'. \tag{10}$$

In liquids and solids, group velocity mismatch, GVM, is important because the pulses walk through each other within the sample [24]. In gases, exciting far from resonances, the GVM is negligible.

3. Experiment

Using the BD technique in which we varied the time delay between and excitation and probe beam, we previously separated the ultrafast and reorientational responses of NLR by exciting

Optics EXPRESS

in the NIR and probing in the visible [10]. Using different methods, others have excited in the near to Mid-IR and probed from the visible to near IR [15,16]. Here, we measure the bound-electronic response in the Mid-IR. We performed three sets of measurements. For the first two sets, we excited at 0.8 μm and probed at 2.4 μm and 3.3 μm. These results are complementary to the measurements of [15,16], where the excitation beams were in the Mid-IR and the probe was at 400–750 nm, since $n_{2,el}(\lambda_p;\lambda_e)$ can be shown to equal $n_{2,el}(\lambda_e;\lambda_p)$. For the third set of measurements, we excited at 3.5 μm and probed at 2.5 μm. While a probe wavelength closer to 3.5 μm would have been desirable to measure the degenerate NLR, this nearly degenerate probe allows spectral blocking of the scattered excitation beam at the probe detector.

We used a commercial Ti:Sapphire laser system (Coherent Legend Elite Duo HE+) to generate 0.8 μm with ~40 fs (FWHM) pulsewidth at a 1 kHz repetition rate. We used part of this 0.8 μm beam for the NIR excitation experiments. For Mid-IR excitation, we used the signal and idler of an optical parametric amplifier (Light Conversion, HE-TOPAS) to generate 3.5 μm using a non-collinear difference frequency generator (NDFG, Light Conversion). To generate probe wavelengths at 2.4 μm and 2.5 μm, we used the idler of an optical parametric amplifier (Light Conversion, TOPAS-Prime). Finally, for generation of the probe beam at 3.3 μm, we generated the difference frequency of the signal and idler output of the TOPAS-Prime using a $AgGaS_2$ crystal. Figure 1 shows the BD setup. The excitation beam creates an index gradient that deflects the weak probe beam in the vertical direction on the quad-cell detector placed in the far field. The beams cross in the horizontal plane and the probe is vertically displaced from the center of the Gaussian excitation beam where it experiences the maximum irradiance gradient. In all experiments, the excitation beam was focused to a spot size more than 3 times larger than that of the probe. The energy difference between the top and bottom segments of the detector, when normalized to the total transmitted probe energy ($\Delta E/E$), is directly proportional to the change of refractive index [18]. In this experiment, we used a mercury cadmium telluride (MCT) quad-cell detector custom-made by Infrared System Associates, Inc., to measure the deflection of the probe in the Mid-IR.

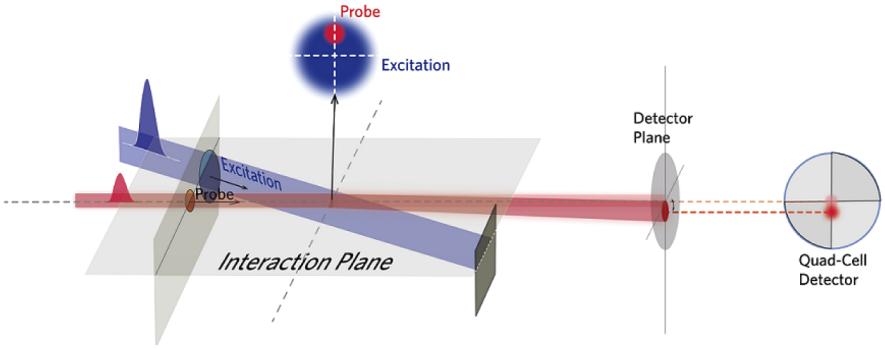

Fig. 1. Beam-Deflection-experimental setup for measuring the deflection of the time-delayed probe (red) due to excitation (blue) with probe displaced from the center of the excitation. The photodetector gives the difference of the voltage on top and bottom halves of segments of the quad cell detector, proportional to ΔE, and their sum, proportional to the total transmitted energy, E.

A beam profiling camera, together with slit and knife edge scans, were used to measure the spot sizes of excitation and probe beams for each set of measurements. The 0.8 μm and 3.5 μm excitation beams were focused to 240 μm and 250 μm HW1/e^2M respectively. The 2.4 μm, 2.5 μm, and 3.3 μm probe beams were focused to 69 μm, 78 μm, and 75 μm HW1/e^2M, respectively. The pulsewidth of the 0.8 μm excitation pulse was measured using a GRENOUILLE

Optics EXPRESS

[37] device as 69 fs (FWHM). The 2.4 μm and 3.3 μm pulsewidths were then measured to be 240 fs and 180 fs (FWHM) by cross-correlation with the 0.8 μm pulse using BD in fused silica. For fitting the overall temporal response, it is the convolution of the full response function with the cross-correlation of the excitation and probe pulses that is important [36], and not the individual pulsewidths. For the ultrafast bound-electronic response, the response function is simply a delta function (again this ignores the small vibrational Raman contribution - see Sec. 6); however, for determining $n_{2,el}$ relative to $\Delta\alpha$ values from Eq. (8), the molecular reorientational response function is needed. We have performed the above-described integrals numerically, and this is what is shown in the following plots of signal versus time delay (e.g., Figs. 2, 3 and 5). The cross correlation of the 3.5 μm and 2.5 μm pulses was measured by BD in BaF_2 as 330 fs, which was corroborated by the BD measurements in air.

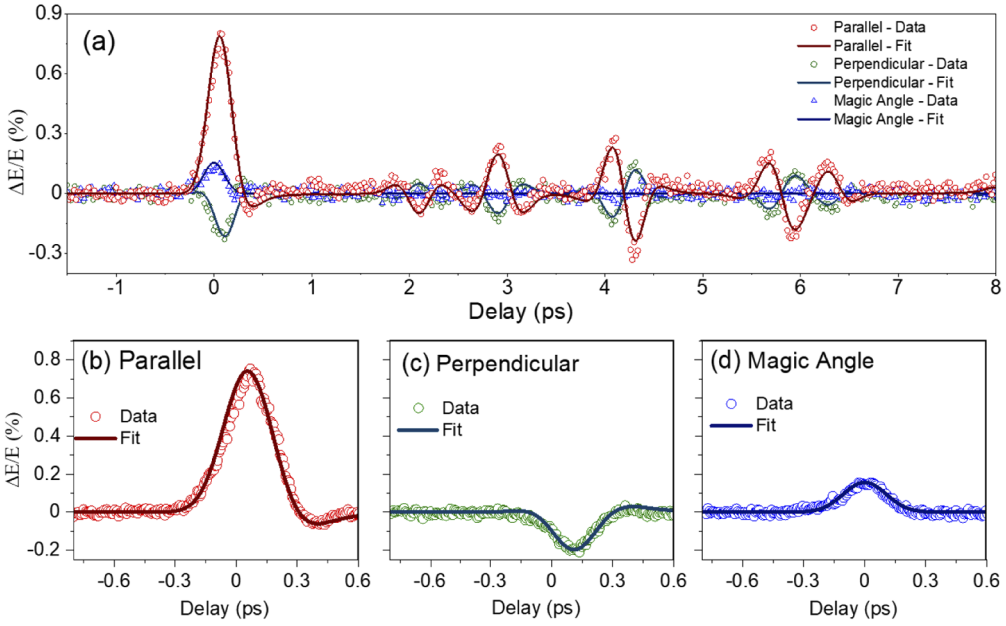

Fig. 2. (a) BD signal using 2.4 μm probe and 0.8 μm excitation in ambient air. Open symbols are data and the solid lines are numerical fits for parallel (red), perpendicular (green), and magic angle (blue) polarization combinations. Bottom figures show scans around zero delay for parallel (b), perpendicular (c) and magic angle (d) polarizations with their respective numerical fits. Solid lines are the corresponding numerical fits for each polarization combination.

We note here that all of our measurements were performed at irradiance levels lower than the threshold for white-light generation, which we observed at 0.8 μm to be ~7.4 TW/cm^2. We therefore performed experiments at irradiances at least 0.8 TW/cm^2 below this threshold. To maintain a sufficiently high signal-to-noise ratio (SNR) we used a small angle (~1.5°) between excitation and probe beams in order to increase the overlap and maximize the signal ($\Delta E/E$). We also used synchronous detection, modulating the excitation beam at 285 Hz, and using a 3 ms integration time, as well as repeating the experiments six times and averaging the results.

For excitation in the Mid-IR, the DFG output energy was insufficient to observe a strong BD signal in ambient air, so we used a pressure cell to increase the molecular density and therefore the SNR. We built a high-pressure chamber using c-axis sapphire windows that transmit Mid-IR wavelengths. The windows were placed far enough from the beam foci to allow high-irradiance in the interaction region without beam overlap at the windows, or producing WLC in the sapphire.

Optics EXPRESS

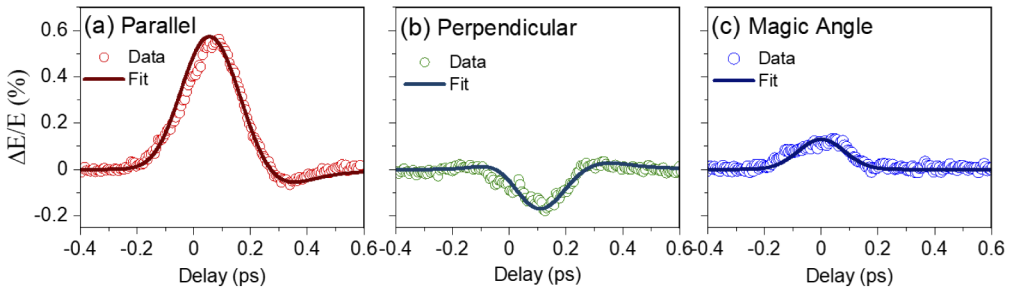

Fig. 3. BD signal using 3.3 μm probe and 0.8 μm in ambient air for parallel (a), perpendicular (b), and magic angle (c) polarization combinations. Solid lines are the corresponding numerical fit for each polarization.

This allowed us to measure these nonlinearities with sufficient SNR to determine the nonlinear response. To reduce the scattering of the excitation beam into the detector we used a larger angle (~3.5°) between excitation and probe beams, which also reduced the signal.

4. Results and discussion

In Fig. 2 we show BD measurements using a 2.4 μm probe and 0.8 μm excitation beam in ambient air. The energy used for the excitation beam was 412 μJ (6.2 TW/cm^2). In order to fit the experimental data we used literature values of the polarizability anisotropy, $\Delta\alpha$, for N_2 and O_2 [11,38] and thus determine the ultrafast $n_{2,el}(\lambda_p;\lambda_e)$ relative to the molecular anisotropy values. The reorientational response for co- and cross-polarized excitation and probe results in index changes of opposite sign. If the angle between excitation and probe polarizations is 54.7° (the so-called magic angle), we obtain zero contribution from the reorientational response [24,39], i.e., as many molecules are rotating toward the angle of polarization of the probe beam as are rotating away. Consequently, we only see the ultrafast bound-electronic response. Figure 2 shows the results for these three polarization combinations. Here we show a long scan including revivals and a scan around zero delay with more points to get better quality fits for $n_{2,el}(\lambda_p;\lambda_e)$. Table 1, shows the values used for all of the numerical fits at normal temperature and pressure conditions (NTP, 20 °C, 1 atm) for rotational constant (B), centrifugal distortion (D) and number density (N) of Nitrogen and Oxygen.

Table 1. Values used in the numerical fits for rotational constant (B), centrifugal distortion (D) and number density (N) at NTP.

	B (m^{-1})	D (m^{-1})	N (m^{-3})
Nitrogen	198.956	5.1×10^{-30}	1.95×10^{25}
Oxygen	143.77	5.9×10^{-30}	0.525×10^{25}

As we mentioned earlier, the dephasing rate Γ changes with pressure [33] and quantum number. We used the values for $\Gamma_{J,J-2}$ given in Ref. [10]. In general, since it is only the response near zero delay that is important for determining $n_{2,el}$, the decay is unimportant; however, at the highest pressure we used in the Mid-IR experiments the decay could be as fast as ~1-2 ps. Including this decay results in an ~4% increase to the $n_{2,el}$ when extrapolated to 1 atm.

The results for a 3.3 μm probe and 0.8 μm excitation in ambient air using an excitation energy of ~ 420 μJ (6.3 TW/cm^2) are shown in Fig. 3 for the three polarization combinations with their respective numerical fits.

Optics EXPRESS

There are two different symmetries involved with bound-electronic (isotropic) and reorientational responses. Any contribution from vibrations is too small to affect our measurements for these pulsewidths. For the isotropic response, $\Delta n_{\parallel}^{el} = 3\Delta n_{\perp}^{el}$ while for a reorientational response $\Delta n_{\parallel}^{rot} = -2\Delta n_{\perp}^{rot}$. Thus, given any two of the polarization combinations, we can calculate the third [17,24]:

$$\begin{aligned} \Delta n(0^\circ) &= \Delta n_{\parallel}^{el} + \Delta n_{\parallel}^{rot} \\ \Delta n(90^\circ) &= \tfrac{1}{3}\Delta n_{\parallel}^{el} - \tfrac{1}{2}\Delta n_{\parallel}^{rot} \\ \Delta n(54.7^\circ) &= \tfrac{5}{9}\Delta n_{\parallel}^{el}. \end{aligned} \tag{11}$$

These relations serve as good checks on the data to ensure proper alignment, overlap and using the correct polarization angles. Figure 4(a) shows the data for a 2.4 μm probe and a 0.8 μm excitation for three polarization combinations in addition to the calculation of each combination using the remaining two combinations. The fits shown in Fig. Figure 3 constrain the values of $n_{2,el}(\lambda_p;\lambda_e)$ to follow Eq. (11). Thus the fit of $n_{2,el}(2.4\ \mu m; 0.8\ \mu m) = (10 \pm 2) \times 10^{-20}\ cm^2/W$ is the best overall fit to the three sets of data around zero delay.

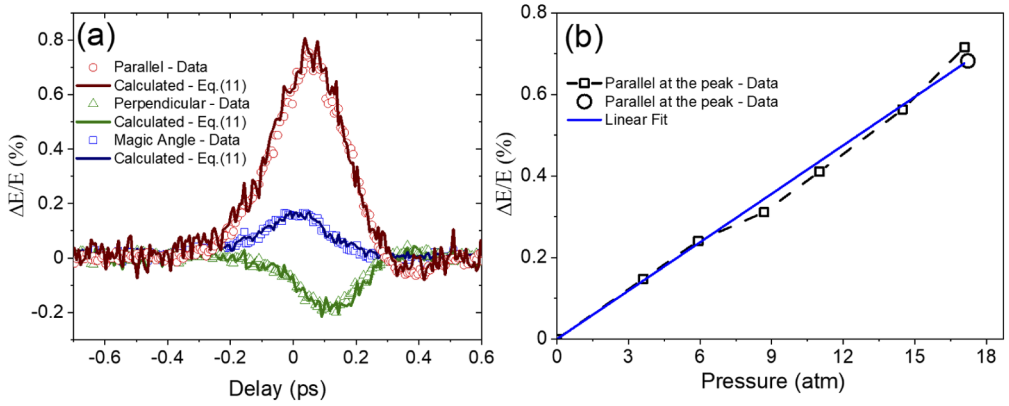

Fig. 4. (a) BD signal versus temporal delay near zero delay using a 2.4 μm probe and 0.8 μm excitation in ambient air for parallel (open red circle), perpendicular (open green triangle), and magic angle (open blue square) using an excitation energy of 412 μJ. The accompanying solid lines (parallel-red, perpendicular-green, and magic angle-blue) were each calculated from the remaining two curves using Eq. (11) as a check on the data. (b) BD signal for parallel polarization at 40.1 μJ excitation energy versus pressure (solid line is a linear fit). The open square data was taken going from high to low pressure and the open circle was taken going back again to high pressure.

We also verified that the nonlinear refractive index scales linearly with pressure (i.e. number density of molecules) [33]. Figure 4(b) shows data looking at the normalized magnitude of the maximum of the first BD peak in the co-polarized geometry shown in (a)as a function of pressure. This maximum includes contributions from the ultrafast and reorientational nonlinearities.

Figure 5 shows the results of an all Mid-IR experiment, exciting with 75 μJ at 3.5 μm and probing at 2.5 μm. We used ultra-zero grade (AI UZ300) dry air with 20-22% O_2 and the remainder N_2 from Airgas Inc. at a pressure of 31.5 atm. Our results, after scaling to 1atm pressure, agree with the ambient air data.

As we saw earlier, the polarization dependence of the BD signal allows separation of the bound-electronic response from the molecular reorientation response, which depends on the polarization anisotropy. However, relatively small variations in $\Delta\alpha$ translate to significant changes in the calculated value for $n_{2,el}(\lambda_p;\lambda_e)$, since the bound-electronic response is proportional to $\Delta\alpha^2$

Optics EXPRESS

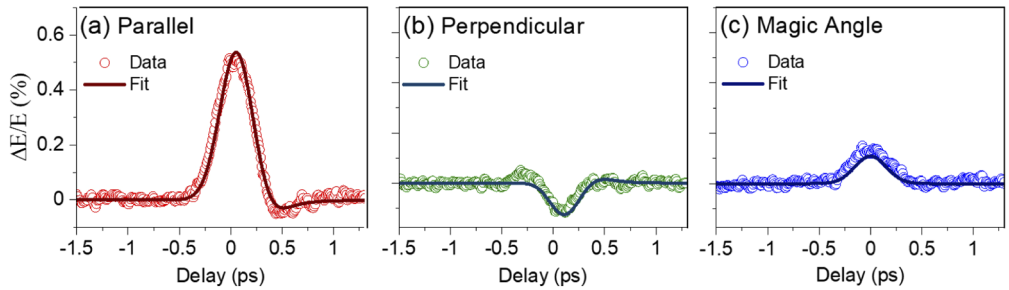

Fig. 5. BD signal for pressurized air at 31.5 atm, exciting at 3.5 µm and probing at 2.5 µm using parallel polarizations (a), perpendicular polarizations (b), and magic angle (c) with their respective numerical fits shown by solid lines.

(Eq. (8)). We fit the data for $n_{2,el}(\lambda_p;\lambda_e)$ using the $\Delta\alpha$ reported by both Bridge and Buckingham [38] and Wahlstrand *et al.* [11].

The second hyperpolarizability (γ) and $n_{2,el}$ for a mixture of molecules is calculated by [10,12]:

$$\gamma_{total} = \sum_i c_i^2 \gamma_i \quad , \quad n_{2,el} = \sum_i c_i n_{2,el}^i \tag{12}$$

where c_i is the percentage of species in the gaseous mixture. For example for air, using $N = 2.5 \times 10^{19}$ cm^{-3} at NTP [40], c_i for N_2, O_2, and Ar are 0.78, 0.21, and 0.01 respectively. In Table 2 we show measured values of $n_{2,el}$ and γ using Eq. (12). Results at higher pressure are scaled to 1 atm.

Table 2. Measured values of $n_{2,el}(\lambda_p;\lambda_e)$ (10^{-20} cm^2/W) and γ (10^{-62} C^{4}m^4/J^3) of air. All values are scaled to 1 atm pressure.

	$\lambda_p(0.65), \lambda_e(0.8)^c$	$\lambda_p(2.4), \lambda_e(0.8)$	$\lambda_p(SC), \lambda_e(2.4)^d$	$\lambda_p(3.3), \lambda_e(0.8)$	$\lambda_p(2.5), \lambda_e(3.5)$
$n_{2,el}(\lambda_p;\lambda_e)^a$	10 ± 2	10 ± 2	9.2 ± 1.4	10± 2	10± 2
$\gamma(\lambda_p;\lambda_e)^a$	1.3 ± 0.3	1.3 ± 0.3	1.2 ± 0.2	1.3 ± 0.3	1.3 ± 0.3
$n_{2,el}(\lambda_p;\lambda_e)^b$	9.0 ± 2.0	9.0 ± 2.0	8.3 ± 1.3	9.0 ± 2.0	9.0 ± 2.0
$\gamma(\lambda_p;\lambda_e)^b$	1.2 ± 0.2	1.2 ± 0.2	1.1 ± 0.2	1.2 ± 0.2	1.2 ± 0.2

[a] value using the $\Delta\alpha$ from [38]
[b] value using the $\Delta\alpha$ from [11]
[c] value reported in [10]
[d] SC – supercontinuum (400-750 nm) from Ref. [16], as calculated from the weighted sum of the air constituents.

In our results we assume NLR due to the molecular reorientation contribution is dispersionless [15,16]. Here as we see in Table 1, we observe no measurable dispersion of the bound-electronic response within our experimental uncertainties. Also, note the agreement between the measurements made with excitation and probe wavelengths switched in the second and third columns which follows the symmetry relation $n_{2,el}(\lambda_p;\lambda_e) = n_{2,el}(\lambda_e;\lambda_p)$.

There are reports of soliton formation in the 3.5 to 4.5 µm range from anomalous dispersion caused by CO_2 ro-vibrational resonances but these would require longer propagation lengths than in our experiments [41,42].

5. Pulsewidth-dependent nonlinear refractive index of air

Knowing the response function Eq. (7), the effective nonlinear refractive index introduced in Eq. (1) for a single beam experiment can be calculated from the response function as follows [24]:

$$n_{2,eff} = n_{2,el} + \frac{\int_{-\infty}^{\infty} I(t) \int_{-\infty}^{\infty} R_{rot}(t-t')I(t')dt'dt}{\int_{-\infty}^{\infty} I^2(t)\,dt}. \tag{13}$$

Optics EXPRESS

We observe that $R_{rot}(t)$ is wavelength independent and thus our results also show that $n_{2,el}$ is wavelength-independent in the near to Mid-IR. Now, from the $R_{rot}(t)$ shown in Fig. 6(a), we are able to predict the pulsewidth dependence for this degenerate $n_{2,eff}$ as is shown in Fig. 6(b), using the values of $\Delta\alpha$ from [11,38].

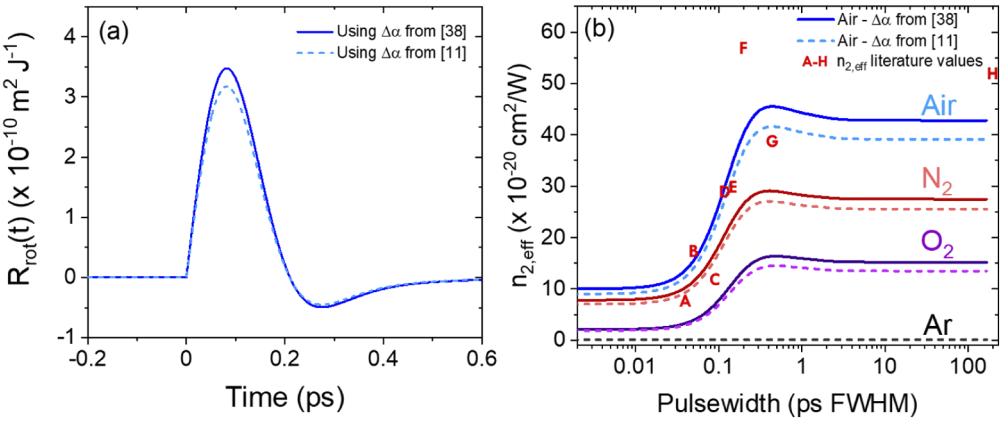

Fig. 6. (a) Response function of air at NTP using Eq. (7) and the values of $\Delta\alpha$ from Ref. [38] (blue solid line) and Ref. [11] (light blue dashed line). (b) Prediction of the pulsewidth dependence of $n_{2,eff}$ for air (blue), N_2 (red), O_2 (purple), and Ar (black) for their respective partial pressures. Solid lines used $\Delta\alpha$ from [38] dashed lines from [11]. The parameters used are given in Table 1 and Table 2. (A-H) indicate measured experimental values of the nonlinear refractive index from [11], [43], [44], [45], [46], [47], [16], and [48], respectively.

Somewhat surprisingly, the resulting curve shown in Fig. 6(b) does not monotonically increase with pulsewidth but exhibits a maximum near ~0.5 ps. This occurs because of the oscillatory shape of the response function, turning negative at longer times. Since Eq. (13) involves a convolution with this oscillatory response function, there are pulsewidths for which the negative contribution lowers the effective nonlinear index.

We also calculated the pulsewidth dependence of the NLR for different pressures as shown in Fig. 7. Both $n_{2,el}$ and Δn_{rot} scale linearly with density N and therefore with pressure P. However, the dephasing rate $\Gamma_{J,J-2}$ also scales linearly with pressure [33] and changes the response function $R_{rot}(t)$, consequently altering the contribution of Δn_{rot} to $n_{2,eff}$. In this analysis we used a different $\Gamma_{J,J-2}$ for each J state as given in Ref. [10] and assumed each gamma scaled linearly with pressure [33]. Figure 7 shows $n_{2,eff}$ for air, N_2, and O_2 normalized such that the bound-electronic responses are the same as at 1 atm. Argon is also included in the sum to give the NLR of air, but is pulsewidth independent since there is no rotational contribution, i.e., $\Delta\alpha$=0. Our results show that for a pressure variation from ~0 atm to 1 atm there is no perceivable change in shape of the scaled $n_{2,eff}$ (see Fig. 7 black solid line and green dashed line). As the pressure is increased further to 35 atm (blue dashed line) and 70 atm (red dotted line) the peak shifts to slightly longer pulsewidths and is suppressed. Our previous studies of the pulsewidth dependence of the nonlinear refraction of a wide variety of molecular liquids [24,25], all showed qualitatively similar curves without a peak, consistent with the trend predicted here.

We can also analyze the effects of temperature on the rotational contribution as shown in Fig. 8. For extremely low temperatures only the lowest rotational state is initially occupied, meaning a single Raman transition is possible, and the rotational response function of each molecular species is a damped sine wave ($\propto \sin(\omega_{j,j-2}(t))e^{-\Gamma_{J,J-2}t}$) according to Eq. (7) (where here, $\omega_{j,j-2}$ is the lowest possible frequency for that species which equals $4\pi cB$). As the temperature is increased, more Raman transitions are possible adding sinusoidal functions of multiples of $4\pi cB$ with the

Optics EXPRESS

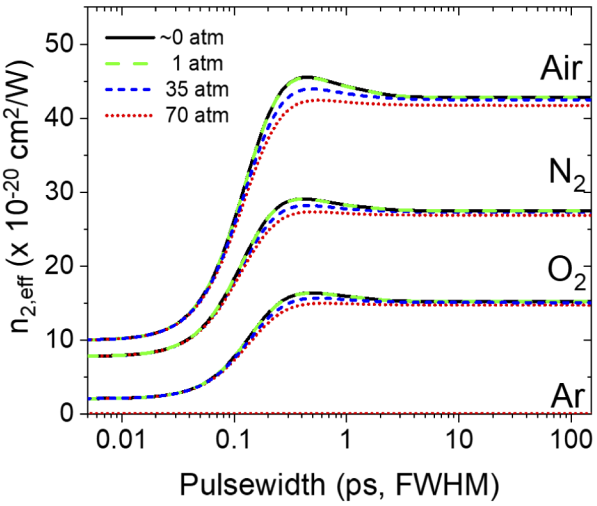

Fig. 7. Pulsewidth dependence of the $n_{2,eff}$ normalized to the $n_{2,el}$ at 1 atm for air and its primary constituents. We show a pressure variation from ~0 atm (black solid line) to 70 atm (red dotted line). The green dashed line corresponds to 1 atm overlapping the black curve for ~0 atm, and the dashed blue line corresponds to 35 atm. All the curves were calculated using the values for $\Delta\alpha$ measured by Bridge *et al.* [38] and $n_{2,el} = 10 \times 10^{-20}$ cm^2/W at NTP.

phase set at time zero by the excitation to add coherently. The weighting factors T_J (see Eq. (5)) combine to keep the initial rise, i.e. slope, of the response from t=0 the same, independent of temperature This is somewhat surprising given the significant changes in weighting factors with temperature; however, for later times the maximum and later oscillations are clearly reduced for higher temperature as expected. Interference of the additional frequencies creates a series of pulses, i.e., revivals, that occur with a period of 1/8cB. These pulses, including the initial pulse near t=0, become shorter as higher frequency Raman transitions are added. This is in analogy to how a modelocked pulse is created except here it has both positive and negative components like the electric field of a modelocked pulse – see Eq. (7). Looking at just the initial response near t=0, at high temperature the addition of sine waves leads to an initial rise to a peak followed by a small negative going peak (note that in contrast to a modelocked pulse, here at time zero, the response is zero, i.e. sine versus cosine). As the temperature is raised from below room temperature to above (see insets of Fig. 8), the increased sum leads to a decrease of both the positive and negative going peaks. In addition, both the initial peak and negative portion move to slightly shorter times as higher frequency Raman terms in the sum are added.

In Fig. 8 we looked at two scenarios; (a) constant N and (b) constant pressure P. When N is constant, as T increases (and thus P also increases) the reorientational response decreases because of the increased collision rate, although this is a relatively small effect. However, at constant P, as T increases (and thus N decreases) both the bound-electronic response and the reorientational response decrease, which results in a much larger overall change to $n_{2,eff}$.

Finally, we analyzed the change of $n_{2,eff}$ for different altitudes in Earth's atmosphere as shown in Fig. 9: sea level, troposphere (10 km altitude), lower stratosphere (20 km altitude), and upper stratosphere (30 km altitude). This prediction is based on the NASA earth atmospheric model [49]. We note that this includes the effects of different temperatures, number densities, and pressures. Changes to the relative concentrations of the primary air constituents for these altitudes are sufficiently small to be inconsequential. Here, sea level corresponds to the NTP conditions.

The changes in $n_{2,eff}$ between different altitudes, plotted on a log-scale in Fig. 9(a), is dominated by differences in the number density. However, when normalized to $n_{2,el}$ at sea level, plotted on a

Optics EXPRESS

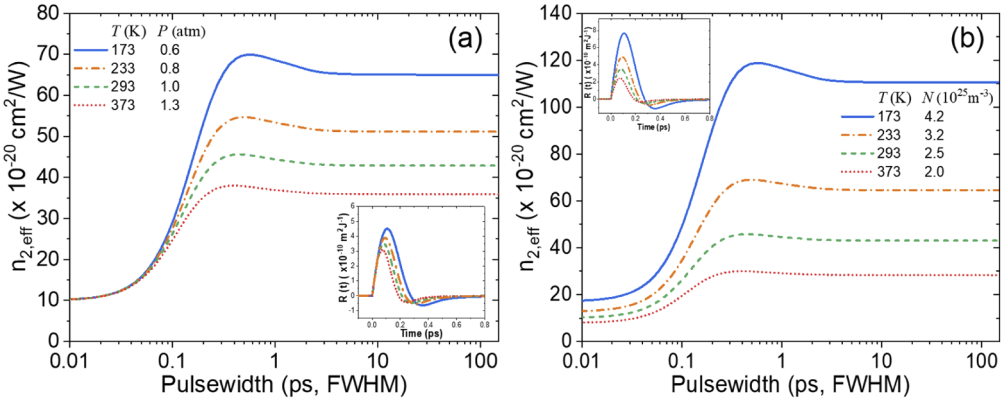

Fig. 8. Effects of temperature changes on $n_{2,eff}$, (a) keeping the number density constant at $N = 2.5 \times 10^{25}$ m^{-3} and (b) keeping the pressure constant at $P = 1$ atm. The insets show the corresponding response functions.

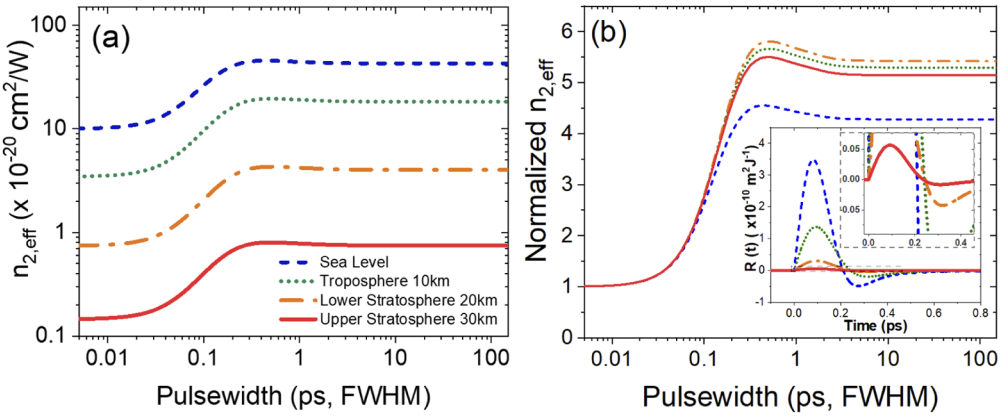

Fig. 9. (a) $n_{2,eff}$ of air at sea level (NTP) in blue dash line (0 km altitude, $P = 1$ atm, $T = 293$ K, $N = 2.5 \times 10^{25}$ m^{-3}), troposphere in green dotted line (10 km altitude, $P = 0.26$ atm, $T = 223$ K, $N = 0.86 \times 10^{25}$ m^{-3}), lower stratosphere in orange dash dotted line (20 km altitude, $P = 0.05$ atm, $T = 216.7$ K, $N = 0.18 \times 10^{25}$ m^{-3}) and upper stratosphere in red solid line (30 km altitude, $P = 0.015$ atm, $T = 232$ K, $N = 0.04 \times 10^{25}$ m^{-3}) [49]. (b) $n_{2,eff}$ normalized to the $n_{2,el}$ at sea level. The inset shows the response function (not normalized) for each case and a zoom-in for upper stratosphere response function.

linear-scale in Fig. 9(b), it can be seen that the peaks remain a nearly constant fraction of the $n_{2,eff}$ in the long-pulsewidth limit, at ~8%, although the peak moves to slightly shorter pulsewidths at higher altitudes. The relative contribution of the rotational nonlinear response increases for higher altitudes due to the lowered temperature and pressure.

6. Effect of the vibrational Raman response

As mentioned earlier, in this paper we have ignored the effects of vibrational Raman. This is justified for pulses longer than ~50 fs since these vibrational Raman transitions are not excited by pulses much longer than the lowest order vibrational transitions of ~1/14 fs for N_2 (Raman shift of 2330 cm^{-1}) and 1/22 fs for O_2 (Raman shift of 1556 cm^{-1}) [14]. However, pulses shorter than this excite the vibrational Raman transitions and alter the overall response function, which is the

Optics EXPRESS

simple sum of the rotational and vibrational components. Zheltikov [50] gives a prescription for calculating this response function and we have included vibrational Raman in our numerical code. At temperatures encountered in the atmosphere, only the ground state is occupied and the selection rules only couple the lowest vibrational states. Using values approximated from Ref. [50] we plot the expected vibrational Raman contribution from air (O_2 plus N_2) in Fig. 10.

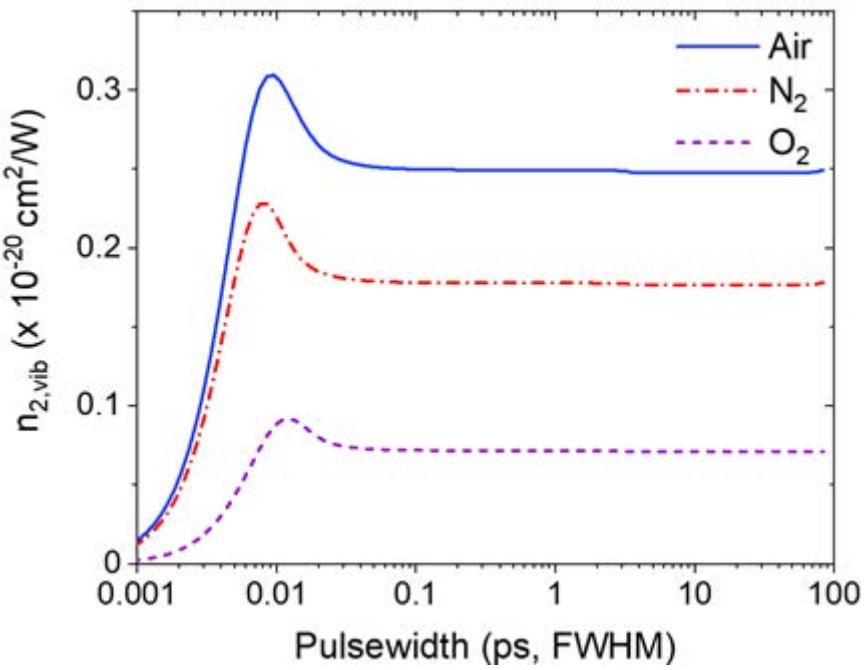

Fig. 10. Vibrational contribution to the $n_{2,eff}$ at NTP based on [50].

These estimated contributions are not significant within our errors. At NTP conditions, this corresponds to ~3% of the bound electronic response for pulses greater than ~10 fs. This is consistent with estimates from [14], and justifies its neglect in multiple previous publications [10,11,13,15,16,44,45,47,48]. Future measurements using extremely short pulses, <10 fs, are needed to confirm our estimates.

7. Conclusions

The NLR of simple molecular gases originates from an almost instantaneous bound-electronic response, a small and ultrafast response due to molecular vibrations, which we ignore and a non-instantaneous reorientational response. As described in Sec. 6 and elsewhere in this paper, we have justified ignoring the small vibrational Raman contribution. The reorientational response, unlike the bound-electronic response, is dependent on the pulsewidth. By using the density matrix formalism, we can determine the reorientational response which, when added to the bound-electronic response, gives the total NLR and thus the effective nonlinear refractive index, $n_{2,eff}$.

Using the polarization sensitive, time-resolved Beam-Deflection technique we performed several sets of measurements by exciting in the NIR and Mid-IR and probing in the Mid-IR to determine the nonlinear refraction in air. Since the bound-electronic and reorientational responses have different symmetries, these effects can be separated using different combinations of excitation and probe polarizations. For this reason we performed different measurements for

Optics EXPRESS

co-polarized, cross-polarized and magic-angle polarizations. The latter polarization sees no contribution from the reorientational response enabling us to find an unambiguous value for the bound-electronic NLR. However, we again point out that we have ignored the vibrational Raman contribution that is predicted to be very small, only reaching appreciable values of ~3% of the bound-electronic contribution for pulsewidths $\gtrsim$ 5 fs.

With the assumption of no dispersion of the molecular reorientational nonlinear response [15,16], we obtain measurements of the nondegenerate bound-electronic nonlinear refractive index, $n_{2,el}(\lambda_p;\lambda_e)$. Previous work has reported nondegenerate measurements with excitation in the visible to Mid-IR with probes in the visible to near-IR [10,15,16,51,52]; however, to our knowledge, there are no previous measurements of near degenerate values in the Mid-IR. This may be due to SNR/sensitivity issues, as measurement sensitivity scales as λ^{-1}. This scaling is also true for Beam Deflection [17], but the sensitivity of BD is high, and combining this with the use of high pressure and our custom-built MCT quad cell gives sufficient SNR for these measurements with both excitation and probe in the Mid-IR. Using the MCT detector and the BD technique we were able to obtain a SNR of unity for an optical path length change of $\lambda/27,000$ (replace λ by 2π for phase shift) for our (2.4 μm; 0.8 μm) measurements and $\lambda/10,000$ for our (2.5 μm; 3.5 μm) measurements.

Our experimental results together with our previous measurements using NIR excitation and visible probe [10] along with other literature data [11,15,16], show no measurable dispersion of the bound-electronic response. The nondegenerate $n_{2,el}(\lambda_p;\lambda_e)$ is connected to 2-photon absorption (2PA) via Kramers-Kronig relations in a way similar to how linear refraction is related to linear absorption [21,53], as has been demonstrated experimentally in a number of solids [53–55]. Similarly, the dispersion in gases should follow the same rules. Since the electronic resonances of all the major constituents of air are in the ultraviolet, the dispersion of $n_{2,el}(\lambda_p;\lambda_e)$ in the near to Mid-IR is expected to be quite small, as these measurements confirm.

In this paper we also present a prediction using Eq. (13) for the effective NLR in air as well as oxygen and nitrogen for different pulsewidths. Since we see no dispersion in the nonlinear refraction, we can determine the pulsewidth, temperature and pressure dependence for all wavelengths in the near to Mid-IR. Our calculations show that the effective NLR is nearly pulsewidth independent for pulsewidths less than ~10 fs. For increasing pulsewidths the effective NLR increases to a maximum at around ~0.5 ps. After a small downturn, further increases in pulsewidth have no effect, i.e., a pulsewidth-independent NLR. We attribute the unusual shape of $n_{2,eff}$ around 0.5 ps pulsewidth to the oscillatory shape of the response function. The effect of increasing the pressure of the gas on $n_{2,eff}$ is to suppress the small maximum around 0.5 ps, which is consistent with our observations in liquids which show no peak [24,25]. Lowering the temperature results in an increased rotational contribution to $n_{2,eff}$ with a more pronounced peak. We also make the technologically important predictions of the nonlinear response of air at different altitudes and temperatures. Below 1 atm, $n_{2,eff}$ is linearly dependent on pressure with no change in the shape of the pulsewidth dependence, although the shape is still temperature dependent.

Funding. Defense Advanced Research Projects Agency (HR0011-17-1-0003); University of Central Florida, College of Graduate Studies (Pre-eminent Postdoctoral Program).

Acknowledgements. This work was supported by DARPA, Defense Advance Project Agency (HR0011-17-1-0003). NM acknowledges UCF Pre-eminent Postdoctoral Program for funding. We also thank Andrew Duran of Infrared Systems Development for design and optimizing the operation of the MCT quad cell detector. We also thank Munan Gao for his help in testing and optimizing the MCT quadcell detector, and Yingjie Chai for Fig. 1. We also thank Prof. David Shelton from the University of Nevada, Las Vegas, for illuminating conversations. Article processing charges were provided in part by the UCF College of Graduate Studies Open Access Publishing Fund.

Disclosures. The authors declare no conflicts of interest.

References

Optics EXPRESS

1. D. K. Killinger, J. H. Churnside, and L. S. Rothman, "Atmospheric Optics," in *Handbook of Optics Volume I Fundamentals, Techniques, and Design*, M. Bass, E. W. Van Stryland, D. R. Williams, and W. L. Wolfe, eds., 2nd ed. (McGraw-Hill, Inc ., 1995).
2. A. V. Mitrofanov, A. A. Voronin, D. A. Sidorov-Biryukov, A. Pugžlys, E. A. Stepanov, G. Andriukaitis, T. Flöry, S. Ališauskas, A. B. Fedotov, A. Baltuška, and A. M. Zheltikov, "Mid-infrared laser filaments in the atmosphere," Sci. Rep. **5**(1), 8368 (2015).
3. P. Panagiotopoulos, P. Whalen, M. Kolesik, and J. V. Moloney, "Super high power mid-infrared femtosecond light bullet," Nat. Photonics **9**(8), 543–548 (2015).
4. H. Liang, D. L. Weerawarne, P. Krogen, R. I. Grynko, C.-J. Lai, B. Shim, F. X. Kärtner, and K.-H. Hong, "Mid-infrared laser filaments in air at a kilohertz repetition rate," Optica **3**(7), 678 (2016).
5. J. Kasparian, "White-Light Filaments for Atmospheric Analysis," Science **301**(5629), 61–64 (2003).
6. S. L. Chin, H. L. Xu, Q. Luo, F. Théberge, W. Liu, J. F. Daigle, Y. Kamali, P. T. Simard, J. Bernhardt, S. A. Hosseini, M. Sharifi, G. Méjean, A. Azarm, C. Marceau, O. Kosareva, V. P. Kandidov, N. Aközbek, A. Becker, G. Roy, P. Mathieu, J. R. Simard, M. Châteauneuf, and J. Dubois, "Filamentation "remote" sensing of chemical and biological agents/pollutants using only one femtosecond laser source," Appl. Phys. B: Lasers Opt. **95**(1), 1–12 (2009).
7. L. Bergé, S. Skupin, R. Nuter, J. Kasparian, and J. P. Wolf, "Ultrashort filaments of light in weakly ionized, optically transparent media," Rep. Prog. Phys. **70**(10), 1633–1713 (2007).
8. B. Shim, S. E. Schrauth, and A. L. Gaeta, "Filamentation in air with ultrashort mid-infrared pulses," Opt. Express **19**(10), 9118 (2011).
9. G. O. Ariunbold, P. Polynkin, and J. V. Moloney, "Third and fifth harmonic generation by tightly focused femtosecond pulses at 22 μm wavelength in air," Opt. Express **20**(2), 1662 (2012).
10. M. Reichert, P. Zhao, J. M. Reed, T. R. Ensley, D. J. Hagan, and E. W. Van Stryland, "Beam deflection measurement of bound-electronic and rotational nonlinear refraction in molecular gases," Opt. Express **23**(17), 22224 (2015).
11. J. K. Wahlstrand, Y. H. Cheng, and H. M. Milchberg, "Absolute measurement of the transient optical nonlinearity in N_2, O_2, N_2O, and Ar," Phys. Rev. A: At., Mol., Opt. Phys. **85**(4), 043820 (2012).
12. D. P. Shelton and J. E. Rice, "Measurements and Calculations of the Hyperpolarizabilities of Atoms and Small Molecules in the Gas Phase," Chem. Rev. **94**(1), 3–29 (1994).
13. J. J. Pigeon, S. Y. Tochitsky, E. C. Welch, and C. Joshi, "Measurements of the nonlinear refractive index of air, N2, and O2 at 10 μm using four-wave mixing," Opt. Lett. **41**(17), 3924 (2016).
14. D. P. Shelton, "Vibrational contributions to the hyperpolarizabilities of homonuclear diatomic molecules," Mol. Phys. **60**(1), 65–76 (1987).
15. S. Zahedpour, J. K. Wahlstrand, and H. M. Milchberg, "Measurement of the nonlinear refractive index of air constituents at mid-infrared wavelengths," Opt. Lett. **40**(24), 5794 (2015).
16. S. Zahedpour, S. W. Hancock, and H. M. Milchberg, "Ultrashort infrared 2.5–11 μm pulses: spatiotemporal profiles and absolute nonlinear response of air constituents," Opt. Lett. **44**(4), 843 (2019).
17. M. R. Ferdinandus, H. Hu, M. Reichert, D. J. Hagan, and E. W. Van Stryland, "Beam deflection measurement of time and polarization resolved ultrafast nonlinear refraction," Opt. Lett. **38**(18), 3518 (2013).
18. Y.-H. Chen, S. Varma, A. York, and H. M. Milchberg, "Single-shot, space- and time-resolved measurement of rotational wavepacket revivals in H2, D2, N2, O2, and N2O," Opt. Express **15**(18), 11341 (2007).
19. M. A. Spackman, "Time-dependent Hartree-Fock second-order molecular properties with a moderately sized basis set. I. The frequency dependence of the dipole polarizability," J. Chem. Phys. **94**(2), 1288–1294 (1991).
20. G. R. Alms, A. K. Burnham, and W. H. Flygare, "Measurement of the dispersion in polarizability anisotropies," J. Chem. Phys. **63**(8), 3321–3326 (1975).
21. D. C. Hutchings, M. Sheik-Bahae, D. J. Hagan, and E. W. Van Stryland, "Kramers-Krönig relations in nonlinear optics," Opt. Quantum Electron. **24**(1), 1–30 (1992).
22. D. Mcmorrow, W. T. Lotshaw, and G. A. Kenney-Wallace, "Femtosecond Optical Kerr Studies on the Origin of the Nonlinear Responses in Simple Liquids," IEEE J. Quantum Electron. **24**(2), 443–454 (1988).
23. R. K. Raj, D. Bloch, J. J. Snyder, G. Camy, and M. Ducloy, "High-frequency optically heterodyned saturation spectroscopy via resonant degenerate four-wave mixing," Phys. Rev. Lett. **44**(19), 1251–1254 (1980).
24. M. Reichert, H. Hu, M. R. Ferdinandus, M. Seidel, P. Zhao, T. R. Ensley, D. Peceli, J. M. Reed, D. A. Fishman, S. Webster, D. J. Hagan, and E. W. Van Stryland, "Temporal, spectral, and polarization dependence of the nonlinear optical response of carbon disulfide," Optica **1**(6), 436 (2014).
25. P. Zhao, M. Reichert, S. Benis, D. J. Hagan, and E. W. Van Stryland, "Temporal and polarization dependence of the nonlinear optical response of solvents," Optica **5**(5), 583 (2018).
26. C. H. Lin, J. P. Heritage, T. K. Gustafson, R. Y. Chiao, and J. P. McTague, "Birefringence arising from the reorientation of the polarizability anisotropy of molecules in collisionless gases," Phys. Rev. A **13**(2), 813–829 (1976).
27. U. Steinitz, Y. Prior, and I. S. Averbukh, "Optics of a gas of coherently spinning molecules," Phys. Rev. Lett. **112**(1), 013004 (2014).
28. G. Karras, E. Hertz, F. Billard, B. Lavorel, J. M. Hartmann, O. Faucher, E. Gershnabel, Y. Prior, and I. S. Averbukh, "Orientation and alignment echoes," Phys. Rev. Lett. **114**(15), 153601 (2015).
29. C. H. Lin, J. P. Heritage, and T. K. Gustafson, "Susceptibility echos in linear molecular gases," Appl. Phys. Lett. **19**(10), 397–400 (1971).

Optics EXPRESS

30. J. K. Wahlstrand, J. H. Odhner, E. T. McCole, Y. H. Cheng, J. P. Palastro, R. J. Levis, and H. M. Milchberg, "Effect of two-beam coupling in strong-field optical pump-probe experiments," Phys. Rev. A - At. Mol. Opt. Phys. **87**(5), 053801 (2013).
31. E. W. Van Stryland, A. L. Smirl, T. F. Boggess, M. J. Soileau, B. S. Wherrett, and F. A. Hopf, "Weak-Wave Retardation and Phase-Conjugate Self-Defousing in Si," in *Picosecond Phenomena III*., K. B. Eisenthal, R. M. Hochstrasser, W. Kaiser, and A. Laubereau, eds. (Springer Series in Chemical Physics, vol 23., 1982), Vol. 23, pp. 368–371.
32. In ref. [10] the Eq. (2) have a typographical error corrected here in Eq. (4). The reported values are correct.
33. J. D. Miller, S. Roy, J. R. Gord, and T. R. Meyer, "Communication: Time-domain measurement of high-pressure N_2 and O_2 self-broadened linewidths using hybrid femtosecondpicosecond coherent anti-Stokes Raman scattering," J. Chem. Phys. **135**(20), 201104 (2011).
34. L. C. Hoskins, "Pure rotational Raman spectroscopy of diatomic molecules," J. Chem. Educ. **52**(9), 568 (1975).
35. J. C. Diels and W. Rudolph, *Ultrashort Laser Pulse Phenomena*, 2nd editio (Elsevier, 2006).
36. K. Kamada, "Mechanisms of ultrafast refractive index change in organic system," Proc. SPIE **4797**, 65 (2003).
37. R. Trebino, P. O'Shea, M. Kimmel, and X. Gu, "Very Simple FROG Apparatus: GRENOUILLE," in *Frequency-Resolved Optical Gating: The Measurement of Ultrashort Laser Pulses* (Springer US, 2000), pp. 229–236.
38. N. Bridge and A. Buckingham, "The polarization of laser light scattered by gases," Proc. R. Soc. London A **295**(1442), 334–349 (1966).
39. M. Terazima, "Ultrafast transient Kerr lens in solution detected by the dual-beam thermal-lens method," Opt. Lett. **20**(1), 25 (1995).
40. D. R. William, "Earth Fact Sheet," https://nssdc.gsfc.nasa.gov/planetary/factsheet/earthfact.html.
41. A. V. Mitrofanov, A. A. Voronin, M. V. Rozhko, D. A. Sidorov-Biryukov, A. B. Fedotov, A. Pugžlys, V. Shumakova, S. Ališauskas, A. Baltuška, and A. M. Zheltikov, "Self-compression of high-peak-power mid-infrared pulses in anomalously dispersive air," Optica **4**(11), 1405 (2017).
42. A. A. Voronin and A. M. Zheltikov, "Temporal solitons in air," Phys. Rev. A **95**(2), 023826 (2017).
43. D. Thul, M. Richardson, and S. Rostami Fairchild, "Spatially resolved filament wavefront dynamics," Sci. Rep. **10**(1), 8920 (2020).
44. V. Loriot, E. Hertz, O. Faucher, and B. Lavorel, "Measurement of high order Kerr refractive index of major air components," Opt. Express **17**(16), 13429 (2009).
45. E. T. J. Nibbering, G. Grillon, M. A. Franco, B. S. Prade, and A. Mysyrowicz, "Determination of the inertial contribution to the nonlinear refractive index of air, N2, and O2 by use of unfocused high-intensity femtosecond laser pulses," J. Opt. Soc. Am. B **14**(3), 650 (1997).
46. E. T. J. Nibbering, P. F. Curley, G. Grillon, B. S. Prade, M. A. Franco, F. Salin, and A. Mysyrowicz, "Conical emission from self-guided femtosecond pulses in air," Opt. Lett. **21**(1), 62 (1996).
47. A. Börzsönyi, Z. Heiner, M. P. Kalashnikov, A. P. Kovács, and K. Osvay, "Interferometric measurement of nonlinear refractive index of inert gases at various pressures," Opt. InfoBase Conf. Pap. **18**, 25847–25854 (2010).
48. J. J. Pigeon, S. Y. Tochitsky, E. C. Welch, and C. Joshi, "Experimental study of the third-order nonlinearity of atomic and molecular gases using 10-μm laser pulses," Phys. Rev. A **97**(4), 043829 (2018).
49. N. Hall, "Earth Atmosphere Model," https://www.grc.nasa.gov/WWW/K-12/airplane/atmosmet.html.
50. A. M. Zheltikov, "Raman response function of atmospheric air," Opt. Lett. **32**(14), 2052 (2007).
51. S. Tofighi, N. Munera, D. J. Hagan, and E. W. Van Stryland, "Beam Deflection Measurement of Air n2 in Mid-IR," in *Frontiers in Optics + Laser Science APS/DLS* (OSA, 2019), p. JW3A.43.
52. S. Tofighi, N. Munera, M. Gao, D. J. Hagan, and E. W. Van Stryland, "Beam deflection measurements of transient nonlinear refraction in air in the mid-ir," Opt. InfoBase Conf. Pap. Part **F134**, 4–5 (2019).
53. M. Sheik-Bahae, D. C. Hutchings, D. J. Hagan, and E. W. Van Stryland, "Dispersion of bound electron nonlinear refraction in solids," IEEE J. Quantum Electron. **27**(6), 1296–1309 (1991).
54. M. Balu, J. Hales, D. Hagan, and E. Van Stryland, "Dispersion of nonlinear refraction and two-photon absorption using a white-light continuum Z-scan," Opt. Express **13**(10), 3594 (2005).
55. M. Balu, L. A. Padilha, D. J. Hagan, E. W. Van Stryland, S. Yao, K. Belfield, S. Zheng, S. Barlow, and S. Marder, "Broadband Z-scan characterization using a high-spectral-irradiance, high-quality supercontinuum," J. Opt. Soc. Am. B **25**(2), 159 (2008).